IOP PUBLISHING JOURNAL OF PHYSICS D: APPLIED PHYSICS

J. Phys. D: Appl. Phys. **41** (2008) 015302 (9pp) doi:10.1088/0022-3727/41/1/015302

The dielectric properties of charged nanoparticle colloids at radio and microwave frequencies: high frequency relaxation

Shahid Hussain[1] **and Ian J Ford**[2]

[1] Energy and Materials Department, QinetiQ Limited, Cody Technology Park, Farnborough, Hampshire, GU14 0LX, UK
[2] Department of Physics and Astronomy, University College London, Gower Street, London, WC1E 6BT, UK

Received 25 May 2007, in final form 9 October 2007
Published 19 December 2007
Online at stacks.iop.org/JPhysD/41/015302

Abstract
Charged particle colloids typically consist of particles with negative surface charge suspended in an aqueous electrolyte solution, and have been shown to display effective dielectric properties at radio and microwave frequencies which can potentially be tailored for a range of applications. This research describes a model for predicting such properties. A model previously used to account for the dielectric performance at low frequencies is extended to include higher-order terms in angular frequency, ω. The extended model encompasses the high and low frequency relaxation contributions for the dielectric properties of charged particle colloids. The parameters used to tailor these properties are identified.

1. Introduction

Charged particle colloids have been the focus of research for many years [1–3]. The dynamics of the charge distributions within these systems lead to interesting dielectric properties, which occur over a range of timescales determined by various aspects of the system. The motivation of our work stems from the need to explore systems exhibiting losses at radio and microwave frequencies.

Nanoparticle colloids can be incorporated into a range of structures because of their small particle sizes, without significantly affecting mechanical properties such as weight and flexibility. Nanoparticle colloids, with tailored dielectric properties, could potentially be used in a number of applications, such as radar absorbing materials, electromagnetic shielding and tissue imaging [4].

In a previous paper [1], we investigated the dielectric properties of charged nanoparticle colloids at radio and microwave frequencies. There, charged particle colloids were investigated, which consisted of polystyrene particles with negative surface charge, suspended in distilled water at a volume fraction of 0.1. The spherical particle diameters, d, varied from 20 to 220 nm. The results showed the presence of a dielectric loss feature, which was interpreted by fitting to a model. The model consisted of three main contributions, attributed to three different relaxation (energy dissipation) time-dependent processes. The Debye model [4] was used to account for the response of the host medium, water, and the Chassagne *et al* model [5] was used to describe the permittivity response associated with the low frequency relaxation mechanism. The Maxwell–Wagner model was used to model an additional high frequency relaxation contribution not accounted for by the Chassagne *et al* model. The measured dielectric behaviour was well accounted for by the combined contributions of the model.

However, one of the shortcomings of this approach is that it treats the two particle-related relaxation mechanisms separately, with different assumptions used in deriving the two corresponding models. This means that the validity of the two contributions differs depending upon the parameters used. For example, the high frequency relaxation parameters are derived from the Maxwell–Wagner model using the simplification that the double layer forms a thin conducting shell. The Chassagne *et al* model is not restricted by such a simplification and is shown to be valid over a greater range of parameters, including high and low zeta potentials and a greater number

of double layer thicknesses [5]. Therefore, extending the Chassagne *et al* model to account for high frequency, as well as low frequency behaviour, will provide a more comprehensive model to account for the observed behaviour. This paper extends the previous research by describing such a model.

2. Theory

This section describes some of the charge dynamics that lead to the dielectric properties exhibited by charged particle colloids. These are extensively discussed elsewhere [1,2], and so will only be summarized here in the context of the research undertaken.

The response of the colloids to an applied electric field is discussed here in terms of the complex dielectric constant or effective permittivity:

$$\varepsilon(\omega) = \varepsilon'(\omega) - \mathrm{i} \cdot \varepsilon''(\omega), \tag{1}$$

where ε' and ε'' are the real (energy storage) and imaginary (energy loss) components of the effective permittivity, respectively, and ω is the angular frequency.

As stated in section 1, charged particle colloids typically consist of spherical polystyrene particles with negative surface charge (resulting from sulfate surface groups in this case). When such a particle is placed in an aqueous environment, its negative surface charge attracts counter-ions, which leads to the formation of a double layer of charge [2]. The motion of the two types of ions from the bulk electrolyte, when driven by an external oscillating electric field, will therefore be different.

In the absence of an applied electric field, the equilibrium electrostatic potential, φ, is related to the charge density, $\rho(\boldsymbol{r})$, via Poisson's equation:

$$\nabla^2\varphi = -\frac{\rho(\boldsymbol{r})}{\varepsilon}, \tag{2}$$

where the permittivity, $\varepsilon = \varepsilon_r\varepsilon_0$. The charge density is given by

$$\rho(r) = e(z^+n^+(\boldsymbol{r}) - z^-n^-(\boldsymbol{r})), \tag{3}$$

where $n^+(\boldsymbol{r})$ and $n^-(\boldsymbol{r})$ represent the densities of the positive and negative ions, e is the elementary charge and z^+ and z^- are the valences for each of the positive and negative ions.

The positive and negative ion densities are related to the electrostatic potential via Boltzmann's distribution:

$$n^{\pm}(\boldsymbol{r}) = n_0^{\pm}\exp\left(\frac{\pm z^{\pm}e\varphi(\boldsymbol{r})}{kT}\right), \tag{4}$$

where n_0^+ and n_0^- are the positive and negative ion densities in the absence of the potential, k is Boltzmann's constant and T is the temperature.

The equilibrium electrostatic potential is then calculated by solving the resulting Poisson–Boltzmann equation [5], corresponding to zero total current density, $\boldsymbol{j}^{\pm}$, arising from diffusive and field induced motion of the positive and negative ions:

$$\boldsymbol{j}^{\pm} = \pm n^{\pm}(\boldsymbol{r})u\nabla\varphi - D\nabla n^{\pm}(\boldsymbol{r}), \tag{5}$$

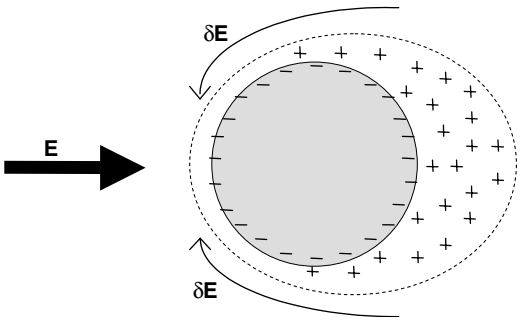

Figure 1. The charge redistribution resulting from the applied field, $\boldsymbol{E}$. The change in dipole strength gives rise to a resultant electric field, $\delta\boldsymbol{E}$.

where u is the mobility and D is the diffusion coefficient of the ions [5].

When a time varying electric field ($\boldsymbol{E} = \boldsymbol{E_0}\mathrm{e}^{\mathrm{i}\omega t}$) is applied to a charged polystyrene particle, the tangential component of the electric field around the particle surface causes azimuthal transport of the double layer ions across the particle. This results in an asymmetric charge distribution in the double layer around the particle, as shown in figure 1. The charge redistribution is accompanied by a change in dipole strength. This gives rise to a resultant electric field, $\delta\boldsymbol{E}$, around the particle, which opposes the applied field as shown in figure 1. The field, $\delta\boldsymbol{E}$, has components tangential and perpendicular to the particle surface [3]. Therefore, the external field-driven charge redistribution will take place tangentially and perpendicularly to the particle surface, which leads to a number of relaxation, or energy dissipating, mechanisms [2].

O'Brien *et al* [3] showed that the tangential and perpendicular flow of counter-ions in the double layer result in a high frequency, low amplitude relaxation (i.e. low energy dissipation), with the relaxation time, τ_1, given by

$$\tau_1 \approx \frac{1}{\kappa^2 D}, \tag{6}$$

where κ is the reciprocal of the double layer thickness and D is the ion diffusivity [5,6].

After this rapid change in the charge density of the double layer, a slower, low frequency, high amplitude, relaxation takes place within the electrolyte, resulting from the changes in the dipole strength of the double layer. The low frequency relaxation time, τ_2, associated with this process is given by

$$\tau_2 = \frac{R^2}{D}, \tag{7}$$

where R is the radius of the particle. The size dependence of this dissipative process is of particular interest here. The relaxation mechanisms are discussed further in [1].

The dielectric dispersion (i.e. frequency dependence of the permittivity) associated with the charge dynamics can be determined by considering the change in electrostatic potential, $\delta\varphi$, and ion densities, $\delta n^{\pm}$, resulting from an applied field, which can be represented as

$$\varphi \to \varphi + \delta\varphi, \tag{8}$$

$$n^{\pm} \to n^{\pm} + \delta n^{\pm}. \tag{9}$$

The continuity of ions is given by

$$\nabla \cdot \boldsymbol{j}^{\pm} + \frac{\partial \delta n^{\pm}}{\partial t} = 0, \tag{10}$$

which leads to two conditions:

$$\nabla \cdot \boldsymbol{j}^{+} + \nabla \cdot \boldsymbol{j}^{-} = -\mathrm{i}\omega(\delta n^{+} + \delta n^{-}), \tag{11}$$

$$\nabla \cdot \boldsymbol{j}^{+} - \nabla \cdot \boldsymbol{j}^{-} = -\mathrm{i}\omega(\delta n^{+} - \delta n^{-}), \tag{12}$$

assuming the density changes are oscillatory and at frequency ω. The changes in electrostatic potential, $\delta\varphi$, and ion densities, $\delta n^{\pm}$, can then be calculated by solving these equations, together with equation (5). Such a solution was obtained by Chassagne *et al* [5], where additional boundary conditions associated with the fields, densities and ion fluxes describing the double layer and the behaviour of the bulk electrolyte far from the particle (asymptotic behaviour) were used. This can then be used to derive an expression for the dipolar coefficient, $\beta(\omega)$. The relationship between $\beta(\omega)$ and permittivity will be given shortly. The Chassagne *et al* model is valid for all double layer thicknesses, κ^{-1} and zeta potentials, ξ (electrostatic potential resulting from double layer ions [7]). The result derived by Chassagne *et al* for the high zeta potential case is presented here (equation (13)). A more detailed description of the parameters used to model this behaviour can be found in [5].

$$\beta(\omega) = \frac{K_2 - K_1 + 2K_{\parallel}^{\mathrm{s}}/R + K_{\perp}^{\mathrm{D}}/R}{K_2 + 2K_1 + 2K_{\parallel}^{\mathrm{s}}/R - 2K_{\perp}^{\mathrm{D}}/R}, \tag{13}$$

where K_1 and K_2 are the frequency-dependent electrolyte and particle complex conductances, respectively, $K_{\parallel}^{\mathrm{s}}$ represents the complex conductance of the double layer along the particle surface, $K_{\perp}^{\mathrm{D}}$ is the perpendicular complex conductance due to the diffusion layer outside the double layer and R is the particle radius. $K_{\parallel}^{\mathrm{s}}$ and $K_{\perp}^{\mathrm{D}}$ are both related to the zeta potential, as shown in equations (14) and (15) [5].

$$K_{\parallel}^{\mathrm{s}} = \frac{-eD}{kT}\left[\left|\frac{q^{\mathrm{s}}\varepsilon_0\varepsilon_1\xi}{R}\right|\right], \tag{14}$$

$$K_{\perp}^{\mathrm{D}} = 2\frac{J_1}{J_2}\frac{eD}{kT}\left[\left|\frac{q^{\mathrm{s}}\varepsilon_0\varepsilon_1\xi}{R}\right|\right], \tag{15}$$

where ε_1 is the electrolyte permittivity, q^{s} is the surface charge density [8] and

$$J_1 = 1 + \lambda_n R \tag{16}$$

$$J_2 = 2 + 2\lambda_n R + \lambda_n^2 R^2 \tag{17}$$

and λ_n^2 is an eigenvalue of a matrix equation describing the behaviour beyond the double layer, as summarized by Chassagne *et al* [5].

The dielectric properties of a colloid can be represented by the complex electric conductivity $K^*(\omega)$:

$$K^*(\omega) = \sigma(\omega) + \mathrm{i}\omega\varepsilon_0\varepsilon'(\omega), \tag{18}$$

where $\sigma(\omega)$ is the frequency-dependent conductivity and $\varepsilon'(\omega)$ is the real permittivity of the colloid.

The dipolar coefficient and complex conductivity are related by the Maxwell–Wagner equation [5]:

$$\frac{K^*(\omega) - K_1}{K^*(\omega) + 2K_1} = V\beta, \tag{19}$$

which, at dilute concentrations, reduces to

$$K^*(\omega) = K_1(1 + 3V\beta), \tag{20}$$

where V is the volume fraction of the particles.

The dipolar coefficient and the permittivity of the charged particle colloids can therefore be related by [6]

$$\frac{\varepsilon'(\omega) - \varepsilon_2}{3V\varepsilon_2} = \beta'(\omega) + \frac{\beta''(\omega)K_1}{\omega\varepsilon_0\varepsilon_1}, \tag{21}$$

$$\frac{\varepsilon''(\omega)}{3V\varepsilon_2} = \frac{(\beta'(\omega) - \beta'(0))K_1}{\omega\varepsilon_0\varepsilon_1} - \beta''(\omega), \tag{22}$$

where ε_1 and ε_2 are the electrolyte and particle permittivity, respectively, β' and β'' are the real and imaginary components of the dipolar coefficient, respectively, and $\varepsilon''(\omega)$ is the imaginary permittivity of the colloid.

Equations (21) and (22) now enable the dielectric properties to be determined, using the zeta potential, ξ, and double layer thickness, κ^{-1}, as fitting parameters. An estimate of ξ and κ^{-1} can also be obtained from equations given in [6, 9]. However, equations (21) and (22) are valid only for frequencies much lower than the relaxation frequency of water [4]. They also do not account for the high frequency relaxation region. This is because the Chassagne *et al* model is valid for frequencies such that $\omega \ll D_{\pm}\kappa^2$ which, as shown in equation (6), is lower than the high frequency relaxation region. The reason for this is that ω is only expanded to first order in the equations shown above [5]. In the previous paper, the contribution to permittivity calculated using this method was referred to as the low frequency contribution, $\varepsilon_{\mathrm{LF}}(\omega)$, (i.e. substituting $\varepsilon(\omega)_{\mathrm{LF}}$ for $\varepsilon(\omega)$ in equations (21) and (22)). The permittivity contribution from the high frequency relaxation, $\varepsilon_{\mathrm{HF}}(\omega)$, was accounted for by the Maxwell–Wagner model, using a method employed by Grosse *et al* [6]. The different relaxation regions were represented by a series of Debye-type contributions, the sum of which provided the overall contribution to permittivity, $\varepsilon_{\mathrm{eff}}(\omega)$:

$$\varepsilon_{\mathrm{eff}}(\omega) = \varepsilon_{\mathrm{LF}}(\omega) + \varepsilon_{\mathrm{HF}}(\omega) + \varepsilon_{\mathrm{wp}} + \varepsilon_{\infty}, \tag{23}$$

ε_{∞} accounts for the permittivity at higher frequencies beyond the relaxation frequency of water, where the permittivity decreases to a constant value (∼4.5 at 20 °C in the case of pure water [4]). The term $\varepsilon_{\mathrm{wp}}$ accounts for the contribution due to water, given by the Debye model [4]:

$$\varepsilon_{\mathrm{wp}} = n^2 + \frac{(\varepsilon_1 - n^2)}{1 + \mathrm{i}\omega_{\tau_{\mathrm{wp}}}}, \tag{24}$$

where n is the refractive index ($n^2 = 1.7$ for water [4]) and τ_{wp} is the dipolar relaxation time, dependent upon the viscosity of water ($\eta = 10^{-3}\,\mathrm{N\,sm^{-3}}$) and the radius, a, of a water molecule ($a = 0.14\,\mathrm{nm}$):

$$\tau_{\mathrm{wp}} = \frac{4\pi a^3\eta}{kT}. \tag{25}$$

As explained in section 1, a more comprehensive model is required, combining the low frequency and high frequency relaxation contributions ($\varepsilon_{\mathrm{LF}}(\omega)$ and $\varepsilon_{\mathrm{HF}}(\omega)$, respectively). The extended model is now derived by following a method analogous to that used by Chassagne *et al* . However, the analysis demonstrated here accounts for contributions at higher frequencies, with the inclusion of higher-order terms in ω, as will be highlighted.

In order to determine the dielectric response resulting from the applied electric field, we first consider the change in ion densities, $\delta n^{\pm}$ or δn_i, in such a system, as introduced by equation (9). As shown by Chassagne *et al*, this is given by

$$\Delta\delta n_i = \frac{\mathrm{i}\omega}{D_i}\delta n_i + \frac{v_i z_i e^2 n_\infty}{\varepsilon_0\varepsilon_1 kT}\sum_j z_j \delta n_j, \tag{26}$$

where i or j refer to the positive (+) or negative (−) ionic species.

Equation (26) can also be written in matrix form to give

$$\Delta\begin{pmatrix}\delta n_+\\ \delta n_-\end{pmatrix} = \begin{bmatrix}\mathrm{i}\omega D_+^{-1}+\kappa_0^2 v_+ z_+^2 & \kappa_0^2 v_+ z_+ z_-\\ \kappa_0^2 v_+ z_+ z_- & \mathrm{i}\omega D_-^{-1}+\kappa_0^2 v_- z_-^2\end{bmatrix} \times\begin{pmatrix}\delta n_+\\ \delta n_-\end{pmatrix}, \tag{27}$$

where $\kappa_0^2 = \kappa^2\sum_i v_i z_i$, z_i are the valences for each of the ions and v_i are the corresponding stoichiometric coefficients.

Using the same terminology as Chassagne *et al*, the eigenvectors of the matrix are designated δn_{n} and δn_c and the corresponding eigenvalues are written λ_n^2 and λ_c^2. These satisfy

$$\Delta\delta n_n = \lambda_n^2\delta n_n \qquad \text{and} \qquad \Delta\delta n_c = \lambda_c^2\delta n_c. \tag{28}$$

The resulting equations are all reduced to first order in ω [O(ω)] by Chassagne *et al*. These equations are then used to obtain the result for the dipolar coefficient, $\beta(\omega)$ (equation (13)). The second order [O(ω^2)] solutions of the resulting equations are summarized in the equations that follow, which have also been extended to third order in the appendix.

In order to obtain the eigenvalues of the matrix shown in equation (27), the corresponding determinantal equation is first solved. Assuming the matrix equation is of the form $\boldsymbol{Ax} = \lambda\boldsymbol{x}$, where $\boldsymbol{A}$ is the matrix:

$$\boldsymbol{A} = \begin{bmatrix}\mathrm{i}\omega D_+^{-1}+\kappa_0^2 v_+ z_+^2 & \kappa_0^2 v_+ z_+ z_-\\ \kappa_0^2 v_+ z_+ z_- & \mathrm{i}\omega D_-^{-1}+\kappa_0^2 v_- z_-^2\end{bmatrix}, \tag{29}$$

the characteristic equation is given by $|\boldsymbol{A}-\lambda\boldsymbol{I}| = 0$:

$$\text{i.e.}\begin{vmatrix}\mathrm{i}\omega D_+^{-1}+\kappa_0^2 v_+ z_+^2-\lambda & \kappa_0^2 v_+ z_+ z_-\\ \kappa_0^2 v_+ z_+ z_- & \mathrm{i}\omega D_-^{-1}+\kappa_0^2 v_- z_-^2-\lambda\end{vmatrix} = 0. \tag{30}$$

This leads to the quadratic equation:

$$\lambda^2 - \lambda(\mathrm{i}\omega D_+^{-1}+\mathrm{i}\omega D_-^{-1}+\kappa_0^2 v_+ z_+^2+\kappa_0^2 v_- z_-^2) - \omega^2 D_+^{-1}D_-^{-1} + \mathrm{i}\omega\kappa_0^2(D_+^{-1}v_- z_-^2 + D_-^{-1}v_+ z_+^2) = 0. \tag{31}$$

The quadratic equation (31) is then solved to give the two eigenvalues λ_n^2 and λ_c^2 of the matrix. These are shown in equations (32) and (33), respectively, with the second order terms [O(ω^2)], resulting from the Taylor expansions, also included.

$$\lambda_n^2 = \mathrm{i}\omega\left(\frac{z_+D_-^{-1}-z_-D_+^{-1}}{z_+-z_-}\right) - \frac{\omega^2(z_-D_+^{-2}-z_+D_-^{-2})}{\kappa^2(z_+-z_-)}, \tag{32}$$

$$\lambda_c^2 = \kappa^2 + \mathrm{i}\omega\left(\frac{z_+D_+^{-1}-z_-D_-^{-1}}{z_+-z_-}\right) + \frac{\omega^2(z_-D_+^{-2}-z_+D_-^{-2})}{\kappa^2(z_+-z_-)}. \tag{33}$$

As expected, the first order terms [O(ω)] shown in equations (32) and (33) are in agreement with those found by Chassagne *et al*.

The eigenvalues can then be used to find the resulting eigenvectors, δn_n and δn_c, which are given by

$$\delta n_c = \delta n_+ - \delta n_-\left[1 - \frac{\mathrm{i}\omega}{\kappa^2}(D_+^{-1}-D_-^{-1}) - \frac{\omega^2(z_-D_+^{-2}-z_+D_-^{-2})}{\kappa^4 z_-}\right], \tag{34}$$

$$\delta n_n = \delta n_+ - \delta n_-\left(\frac{z_+}{z_-}\right)\left[1 + \frac{\mathrm{i}\omega}{\kappa^2}(D_+^{-1}-D_-^{-1}) + \frac{\omega^2(z_-D_+^{-2}-z_+D_-^{-2})}{\kappa^4 z_+}\right]. \tag{35}$$

The eigenvalues and eigenvectors now form the fundamental basis for determining the resulting behaviour.

As shown in equations (8) and (9), an applied field results in a change in electrostatic potential, $\delta\varphi$, and ion densities, $\delta n^{\pm}$. The change in positive and negative ion densities can now be obtained from the eigenvectors, δn_n and δn_c, in equations (34) and (35), to give

$$\delta n_- = (\delta n_c - \delta n_n)\frac{z_-}{z_+-z_-} \times\left[1 - \frac{\mathrm{i}\omega}{\kappa^2}(D_+^{-1}-D_-^{-1})\frac{z_++z_-}{z_+-z_-} + \frac{z_-^2\omega^2}{\kappa^4(z_+-z_-)^2} \times\left(\frac{-2(z_-D_+^{-2}-z_+D_-^{-2})}{z_-} - \frac{z_-(D_+^{-1}-D_-^{-1})^2}{(z_+-z_-)}\left(1+\frac{z_+}{z_-}\right)^2\right)\right], \tag{36}$$

$$\delta n_+ = \frac{1}{z_+-z_-} \times\left[z_+\delta n_c - z_-\delta n_n - \frac{\mathrm{i}\omega}{\kappa^2}(D_+^{-1}-D_-^{-1}) \times\frac{2z_+z_-(\delta n_c-\delta n_n)}{z_+-z_-} + \frac{z_+z_-\omega^2(\delta n_c-\delta n_n)}{\kappa^4(z_+-z_-)^3} \times\left((z_-D_+^{-2}-z_+D_-^{-2})\left(-2(z_+-z_-)+\frac{(z_++z_-)^3}{z_+z_-}\right) \times -(D_+^{-1}-D_-^{-1})^2\left(-\frac{(z_++z_-)(z_+-z_-)^2}{z_-} + z_-^2\left(1+\frac{z_+}{z_-}\right)^2\right)\right)\right]. \tag{37}$$

As shown by Chassagne *et al*, the eigenvector δn_c provides no contribution to the asymptotic solution (solution in the bulk electrolyte beyond double layer). This is because it typically decays over a Debye length ($\sim$double layer thickness, κ^{-1}) due to the contribution of κ^2 in the eigenvalue λ_c^2. The equations for the change in ion densities corresponding to the positive and negative ion densities can therefore be simplified to

$$\delta n_-^{\mathrm{a}} = \frac{-z_-\delta n_n}{z_+ - z_-} \times \left[1 - \frac{\mathrm{i}\omega}{\kappa^2}(D_+^{-1} - D_-^{-1})\frac{z_+ + z_-}{z_+ - z_-} + \frac{z_-^2\omega^2}{\kappa^4(z_+ - z_-)^2} \times \left(\frac{-2(z_-D_+^{-2} - z_+D_-^{-2})}{z_-} - \frac{z_-(D_+^{-1} - D_-^{-1})^2}{(z_+ - z_-)} \left(1 + \frac{z_+}{z_-}\right)^2 \right) \right], \tag{38}$$

$$\delta n_+^{\mathrm{a}} = \frac{-z_-\delta n_n}{z_+ - z_-} \times \left[1 - \frac{\mathrm{i}\omega}{\kappa^2}(D_+^{-1} - D_-^{-1})\frac{2z_+z_-}{z_+ - z_-} + \frac{z_+\omega^2}{\kappa^4(z_+ - z_-)^3} \times \left((z_-D_+^{-2} - z_+D_-^{-2})\left(-2(z_+ - z_-) + \frac{(z_+ - z_-)^3}{z_+z_-}\right) \times \left(-(D_+^{-1} - D_-^{-1})^2\left(-\frac{(z_+ + z_-)(z_+ - z_-)^2}{z_-}\right) + z_-^2\left(1 + \frac{z_+}{z_-}\right)^2 \right) \right) \right], \tag{39}$$

where the superscript, a, denotes the asymptotic solution, far from the particle.

The resulting charge density is then given by $\delta\rho^{\mathrm{a}} = e(z_+\delta n_+^{\mathrm{a}} + z_-\delta n_-^{\mathrm{a}})$ which leads to

$$\delta\rho^{\mathrm{a}} = \frac{-\mathrm{e}z_-\delta n_{\mathrm{n}}}{z_+ - z_-} \times \left[z_+ + z_- - \frac{\mathrm{i}\omega}{\kappa^2}(D_+^{-1} - D_-^{-1})\left(\frac{2z_+^2 + z_+z_- + z_-^2}{z_+ - z_-}\right) + \frac{\omega^2}{\kappa^4(z_+ - z_-)^2} \left((z_-D_+^{-2} - z_+D_-^{-2})\left(-2z_+^2(z_+ - z_-) + \frac{z_+^2(z_+ - z_-)^3}{z_+z_-} - 2z_-^2\right) - (D_+^{-1} - D_-^{-1})^2 \times \left(-\frac{z_+^2(z_+ + z_-)(z_+ - z_-)^2}{z_-} + z_+^2z_-^2\left(1 + \frac{z_+}{z_-}\right)^2 + \frac{z_+^4}{z_+ - z_-}\left(1 + \frac{z_+}{z_-}\right)^2 \right) \right) \right]. \tag{40}$$

The first order terms shown in equation (40) are again in agreement with those given by Chassagne *et al*.

With the extended second order equations shown above, the corresponding asymptotic solution of Poisson's equation beyond the double layer also needs to be corrected. This is given by

$$\delta\psi^{\mathrm{a}} = \left(-E_0r + \frac{P}{4\pi\varepsilon_0\varepsilon_1r^2}\right)\cos\theta + A_n\delta n_n, \tag{41}$$

where r is the radial position.

The first term is accounted for by the external electric field potential. The second term accounts for the change in electric potential associated with the asymptotic dipole field, of strength P. The third term is used by Chassagne *et al* to determine the contribution from the ionic distribution around the sphere. This is given by

$$A_n = \frac{-\delta\rho^{\mathrm{a}}}{\lambda_n^2(z_+ - z_-)\delta n_n\varepsilon_0\varepsilon_1}. \tag{42}$$

The equations derived above can now be used to determine the dipolar coefficient, $\beta(\omega)$, as shown in equation (13). However, the term for the perpendicular complex conductance due to the diffusion layer outside the double layer, $K_\perp^{\mathrm{D}}$, is also adjusted to include second order contributions and is given by

$$\boldsymbol{K}_\perp^{\mathrm{D}} = R\frac{F}{H}, \tag{43}$$

where

$$F = A_n\left[J_1\left(\frac{2}{R}K_\parallel^{\mathrm{s}} + K_2\right) + J_2K_1\right] + \frac{ez_-}{z_+ - z_-}\sum z_iN_i\left(J_1\frac{2D_i^{\mathrm{s}}}{R} - J_2D_i\right), \tag{44}$$

$$D_i^{\mathrm{s}} = D_i\frac{ez_-\xi}{kT\kappa}, \qquad N_i = \frac{\delta n_i(z_+ - z_-)}{(\delta n_c - \delta n_n)z_-} \tag{45}$$

and

$$H = J_2\left[A_n - \frac{z_-}{z_+ - z_-}N_-\frac{kT}{ez_-\nu_-n_\infty}\right]. \tag{46}$$

The permittivity resulting from the extended dipolar coefficient can be calculated from equations (21) and (22). Because this new approach has been applied to determine the high as well as low frequency relaxation behaviour, the resulting permittivity contribution will be referred to as $\varepsilon(\omega)_{\mathrm{HLF}}$. The overall permittivity of the system, $\varepsilon_{\mathrm{eff}\_2}(\omega)$, is now given by

$$\varepsilon_{\mathrm{eff}\_2}(\omega) = \varepsilon_{\mathrm{HLF}}(\omega) + \varepsilon_{\mathrm{wp}} + \varepsilon_\infty. \tag{47}$$

3. Comparison of models

Figures 2 and 3 compare the real and imaginary components of permittivity for results derived from the first model [1] represented by equation (23) ($\varepsilon_{\mathrm{eff}}(\omega)$) and the extended model

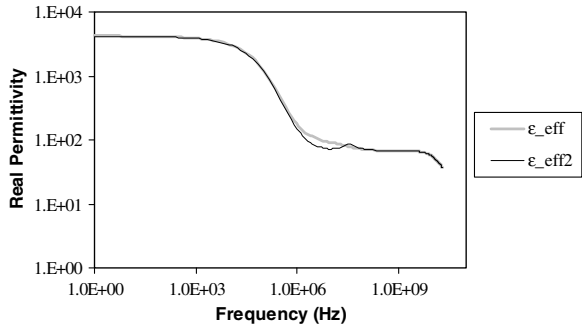

Figure 2. Comparison of predicted real permittivity for 110 nm charged polystyrene colloids ($\xi = 4kT/e$ and $\kappa R = 30$, $D = 1.1 \times 10^{-9}\,\mathrm{m^2\,s^{-1}}$, $T = 298\,\mathrm{K}$, particle (polystyrene) permittivity, $\varepsilon_2 = 2$, electrolyte (water) permittivity, $\varepsilon_1 = 78$, $\varepsilon_\infty = 4.5$, $V = 0.1$, $\eta = 10^{-3}\,\mathrm{N\,s\,m^{-3}}$).

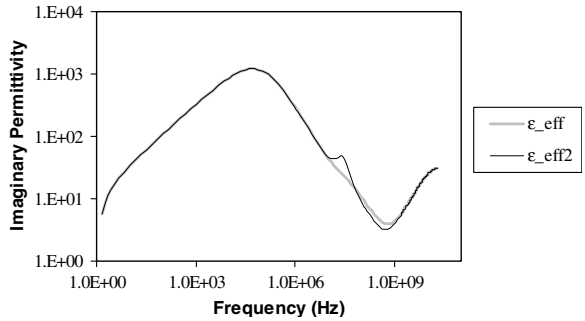

Figure 3. Comparison of predicted imaginary permittivity for 110 nm charged polystyrene colloids ($\xi = 4kT/e$ and $\kappa R = 30$, $D = 1.1 \times 10^{-9}\,\mathrm{m^2\,s^{-1}}$, $T = 298\,\mathrm{K}$, particle (polystyrene) permittivity, $\varepsilon_2 = 2$, electrolyte (water) permittivity, $\varepsilon_1 = 78$, $\varepsilon_\infty = 4.5$, $V = 0.1$, $\eta = 10^{-3}\,\mathrm{N\,s\,m^{-3}}$).

represented by equation (47), with second and third order contributions ($\varepsilon_{\mathrm{eff}\_2}(\omega)$). The performance was modelled using a zeta potential of $\xi = 4kT/e$ (~100 mV) and a value of $\kappa r = 30$. These values were based on previous research [1], where they were estimated from static conductivity measurements on the colloids and shown to produce the best fit to experimental data.

As shown in figures 2 and 3, the two models produce similar performance, with the only change occurring at higher frequencies. Here a small amplitude peak is clearly visible in the extended model results, due to the presence of the higher-order terms highlighted in the equations above. As discussed in section 2, the results of the first model, $\varepsilon_{\mathrm{eff}}(\omega)$, also contain a high frequency relaxation peak (Maxwell–Wagner contribution), which is not observed in figures 2 and 3, due to the low amplitude of the peak in comparison with the relatively high permittivity background medium.

In order to determine the origin of the high frequency peak introduced by the extended model, $\varepsilon_{\mathrm{eff}\_2}(\omega)$, figures 4 and 5 compare the permittivity response at two different particle sizes.

As shown in figures 4 and 5, a decrease in particle size leads to an increase in frequency for the high frequency small amplitude peak. This change in frequency with particle size

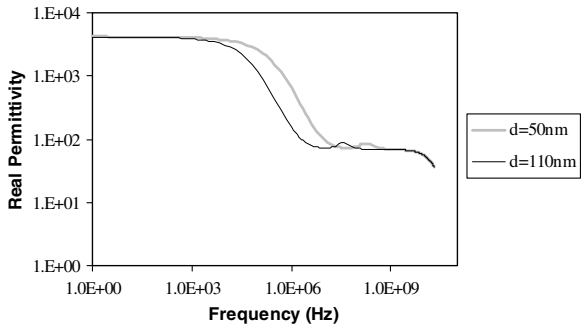

Figure 4. Variation of predicted real permittivity with particle size using extended model (equation (47)).

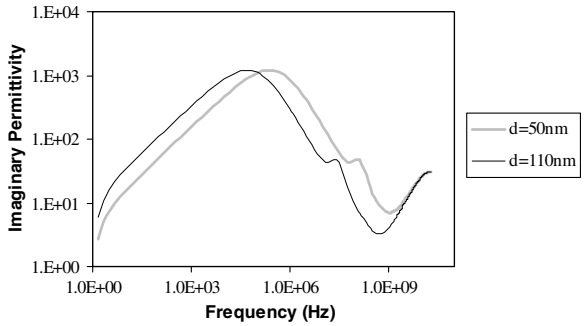

Figure 5. Variation of predicted imaginary permittivity with particle size using extended model (equation (47)).

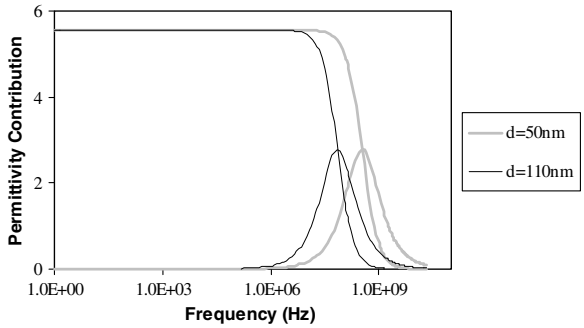

Figure 6. Variation of Maxwell–Wagner permittivity contribution (real and imaginary components) with particle size in model 1 (equation (23)).

is in agreement with that expected from the Maxwell–Wagner equation for the high frequency relaxation response. The high frequency Maxwell–Wagner contributions, $\varepsilon_{\mathrm{HF}}(\omega)$, made to the first model (equation (23)), are shown in figure 6 for the same parameters introduced above.

Figure 6 confirms that the additional high frequency peaks produced by the extended model, $\varepsilon_{\mathrm{eff}\_2}(\omega)$, occur at similar frequencies to those of the high frequency relaxation, with the shifts in frequency with particle size also in agreement. The differences in amplitudes can be explained by differences in the parameters and assumptions used in deriving the two models outlined above.

Although the magnitude of the peak is relatively low, its high frequency position could prove effective for applications operating close to the microwave frequency region, such as microwave absorbers, electromagnetic control and screening applications. For microwave absorbers, minimizing the real component of permittivity, while maximizing the imaginary component is generally desirable [10]. The relatively low real component of permittivity exhibited by high frequency relaxation peak is therefore well suited to such applications. Further optimization of the colloids could be expected by using a lower permittivity background medium, which could result in the relative amplitude of the peak increasing.

4. Conclusion

The inclusion of second and third order terms in angular frequency, ω, has resulted in a model that encompasses both the high and low frequency relaxation contributions for the dielectric properties of charged particle colloids. This represents an improvement on the previous model [1], which treated the mechanisms operating in the two regions separately, with the validity of the solutions obtained restricted by the simplification that the double layer formed a thin conducting shell. The extended model shows a similar response to the previous model at low frequencies. Beyond this region, the extended model shows a larger contribution from the high frequency relaxation, but is still small in comparison with the low frequency, high amplitude relaxation peak. However, this could prove advantageous for applications such as microwave absorbers, where lower real components of permittivity are generally desirable. The extended model is likely to provide broader applicability for the future optimization of such colloids at higher frequencies, because it overcomes the restrictions imposed by the Maxwell–Wagner model. Because of the high frequency position of this peak, it is potentially an important region for applications operating close to the microwave frequency region, such as electromagnetic control and screening applications, and its optimization could therefore prove beneficial in such systems.

Appendix. Extended third order equations

This section presents the extended third order solutions to the equations shown in section 2.

Equations (A32) to (A40) correspond to equations (32)–(40) in section 2, with the additional third order contributions included.

$$\lambda_n^2 = \mathrm{i}\omega\left(\frac{z_+D_-^{-1} - z_-D_+^{-1}}{z_+ - z_-}\right) - \frac{\omega^2(z_-D_+^{-2} - z_+D_-^{-2})}{\kappa^2(z_+ - z_-)} + \frac{\mathrm{i}\omega^3(D_+ + D_-)(z_-D_-^2 - z_+D_+^2)}{\kappa^4 D_+^3 D_-^3(z_+ - z_-)}, \tag{A32}$$

$$\lambda_c^2 = \kappa^2 + \mathrm{i}\omega\left(\frac{z_+D_+^{-1} - z_-D_-^{-1}}{z_+ - z_-}\right) + \frac{\omega^2(z_-D_+^{-2} - z_+D_-^{-2})}{\kappa^2(z_+ - z_-)} - \frac{\mathrm{i}\omega^3(D_+ + D_-)(z_-D_-^2 - z_+D_+^2)}{\kappa^4 D_+^3 D_-^3(z_+ - z_-)}, \tag{A33}$$

$$\delta n_c = \delta n_+ - \delta n_-\left[1 - \frac{\mathrm{i}\omega}{\kappa^2}(D_+^{-1} - D_-^{-1}) - \frac{\omega^2(z_-D_+^{-2} - z_+D_-^{-2})}{\kappa^4 z_-} + \frac{\mathrm{i}\omega^3(D_+ + D_-)(z_-D_-^2 - z_+D_+^2)}{\kappa^6 D_+^3 D_-^3 z_-}\right] \tag{A34}$$

$$\delta n_n = \delta n_+ - \delta n_-\left(\frac{z_+}{z_-}\right)\left[1 + \frac{\mathrm{i}\omega}{\kappa^2}(D_+^{-1} - D_-^{-1}) + \frac{\omega^2(z_-D_+^{-2} - z_+D_-^{-2})}{\kappa^4 z_+} - \frac{\mathrm{i}\omega^3(D_+ + D_-)(z_-D_-^2 - z_+D_+^2)}{\kappa^6 D_+^3 D_-^3 z_+}\right], \tag{A35}$$

$$\begin{aligned}\delta n_- = (\delta n_c - \delta n_n)\frac{z_-}{z_+ - z_-}\Bigg[&1 - \frac{\mathrm{i}\omega}{\kappa^2}(D_+^{-1} - D_-^{-1})\frac{z_+ + z_-}{z_+ - z_-} + \frac{z_-^2\omega^2}{\kappa^4(z_+ - z_-)^2} \\ &\times\left(\frac{-2(z_-D_+^{-2} - z_+D_-^{-2})}{z_-} - \frac{z_-(D_+^{-1} - D_-^{-1})^2}{(z_+ - z_-)}\left(1 + \frac{z_+}{z_-}\right)^2\right) \\ &+\frac{\mathrm{i}\omega^3}{\kappa^6}\left(\frac{-2(D_+ + D_-)(z_-D_-^2 - z_+D_+^2)}{D_+^3D_-^3(z_- - z_+)} + \frac{2(D_- - D_+)(z_- + z_+)(z_-D_-^2 - z_+D_+^2)}{D_+^3D_-^3(z_- - z_+)}\right) \\ &-\frac{z_-(D_+^{-1} - D_-^{-1})(z_- + z_+)\left(-2D_+^{-2} - \dfrac{2z_+D_-^{-2}}{z_-} + \dfrac{(D_+ - D_-)^2(z_- + z_+)^2}{z_-(z_- - z_+)D_+^2D_-^2}\right)}{(-z_- + z_+)^2}\Bigg],\end{aligned} \tag{A36}$$

$$\delta n_+ = \frac{1}{z_+ - z_-}$$

$$\times \left[\begin{array}{l} z_+\delta n_c - z_-\delta n_n - \dfrac{\mathrm{i}\omega}{\kappa^2}(D_+^{-1} - D_-^{-1})\dfrac{2z_+z_-(\delta n_c - \delta n_n)}{z_+ - z_-} + \dfrac{z_+z_-\omega^2(\delta n_c - \delta n_n)}{\kappa^4(z_+ - z_-)^3} \\ \quad \times \left(\begin{array}{l} (z_-D_+^{-2} - z_+D_-^{-2})\left(-2(z_+ - z_-) + \dfrac{(z_+ - z_-)^3}{z_+z_-}\right) \\ \quad -(D_+^{-1} - D_-^{-1})^2\left(-\dfrac{(z_+ + z_-)(z_+ - z_-)^2}{z_-} + z_-^2\left(1 + \dfrac{z_+}{z_-}\right)^2\right) \end{array} \right) \\ -\dfrac{\mathrm{i}\omega^3(\delta n_c - \delta n_n)}{\kappa^6 D_+^3 D_-^3(z_- - z_+)} \left[\begin{array}{l} (z_-D_-^2 - z_+D_+^2)((D_+ - D_-)(z_- + z_+) - (D_- - D_+)(z_- - z_+)) \\ \quad + \dfrac{(D_- - D_+)z_+\left(\dfrac{z_-(D_- - D_+)^2(z_- + z_+)^2}{z_- - z_+} - 2z_-(z_-D_-^2 - z_+D_+^2)\right)}{z_-} \\ \quad + z_+\left(\begin{array}{l} 2(z_-D_-^2 - z_+D_+^2)\left((D_- + D_+) + \dfrac{(D_- - D_+)(z_- + z_+)}{z_+ - z_-}\right) \\ \quad -\dfrac{(D_- - D_+)(z_- + z_+)\left(\dfrac{-z_-(D_- - D_+)^2(z_- + z_+)^2}{z_- - z_+} + 2z_-^2(z_-D_-^2 - z_+D_+^2)\right)}{z_-(z_- - z_+)} \end{array} \right) \end{array} \right] \end{array} \right], \tag{A37}$$

$$\delta n_-^{\mathrm{a}} = \frac{-z_-\delta n_n}{z_+ - z_-} \left[\begin{array}{l} 1 - \dfrac{\mathrm{i}\omega}{\kappa^2}(D_+^{-1} - D_-^{-1})\dfrac{z_+ + z_-}{z_+ - z_-} + \dfrac{z_-^2\omega^2}{\kappa^4(z_+ - z_-)^2}\left(\dfrac{-2(z_-D_+^{-2} - z_+D_-^{-2})}{z_-} - \dfrac{z_-(D_+^{-1} - D_-^{-1})^2}{(z_+ - z_-)}\left(1 + \dfrac{z_+}{z_-}\right)^2\right) \\ \quad + \dfrac{\mathrm{i}\omega^3}{\kappa^6}\left(\dfrac{-2(D_+ + D_-)(z_-D_-^2 - z_+D_+^2)}{D_+^3D_-^3(z_- - z_+)} + \dfrac{2(D_- - D_+)(z_- + z_+)(z_-D_-^2 - z_+D_+^2)}{D_+^3D_-^3(z_- - z_+)}\right) \\ \quad - \dfrac{z_-(D_+^{-1} - D_-^{-1})(z_- + z_+)\left(-2D_+^{-2} - \dfrac{2z_+D_-^{-2}}{z_-} + \dfrac{(D_+ - D_-)^2(z_- + z_+)^2}{z_-(z_- - z_+)D_+^2D_-^2}\right)}{(-z_- + z_+)^2} \end{array} \right], \tag{A38}$$

$$\delta n_+^{\mathrm{a}} = \frac{-z_-\delta n_n}{z_+ - z_-}$$

$$\times \left[\begin{array}{l} 1 - \dfrac{\mathrm{i}\omega}{\kappa^2}(D_+^{-1} - D_-^{-1})\dfrac{2z_+z_-}{z_+ - z_-} + \dfrac{z_+\omega^2}{\kappa^4(z_+ - z_-)^3}\left(\begin{array}{l} (z_-D_+^{-2} - z_+D_-^{-2})\left(-2(z_+ - z_-) + \dfrac{(z_+ - z_-)^3}{z_+z_-}\right) \\ \quad -(D_+^{-1} - D_-^{-1})^2\left(-\dfrac{(z_+ + z_-)(z_+ - z_-)^2}{z_-} + z_-^2\left(1 + \dfrac{z_+}{z_-}\right)^2\right) \end{array} \right) \\ -\dfrac{\mathrm{i}\omega^3}{\kappa^6 D_+^3 D_-^3 z_-(z_- - z_+)} \left[\begin{array}{l} (z_-D_-^2 - z_+D_+^2)((D_+ - D_-)(z_- + z_+) - (D_- - D_+)(z_- - z_+)) \\ \quad + \dfrac{(D_- - D_+)z_+\left(\dfrac{z_-(D_- - D_+)^2(z_- + z_+)^2}{z_- - z_+} - 2z_-(z_-D_-^2 - z_+D_+^2)\right)}{z_-} \\ \quad + z_+\left(\begin{array}{l} 2(z_-D_-^2 - z_+D_+^2)\left((D_- + D_+) + \dfrac{(D_- - D_+)(z_- + z_+)}{z_+ - z_-}\right) \\ \quad -\dfrac{(D_- - D_+)(z_- + z_+)\left(\dfrac{-z_-(D_- - D_+)^2(z_- + z_+)^2}{z_- - z_+} + 2z_-^2(z_-D_-^2 - z_+D_+^2)\right)}{z_-(z_- - z_+)} \end{array} \right) \end{array} \right] \end{array} \right], \tag{A39}$$

$$\delta\rho^{\mathrm{a}} = \frac{-ez_-\delta n_n}{z_+ - z_-}$$

$$\times \left[\begin{array}{l} z_+ + z_- - \dfrac{\mathrm{i}\omega}{\kappa^2}(D_+^{-1} - D_-^{-1})\left(\dfrac{2z_+^2 + z_+z_- + z_-^2}{z_+ - z_-}\right) \\ \quad + \dfrac{\omega^2}{\kappa^4(z_+ - z_-)^2}\left(\begin{array}{l} (z_-D_+^{-2} - z_+D_-^{-2})\left(-2z_+^2(z_+ - z_-) + \dfrac{z_+^2(z_+ - z_-)^3}{z_+z_-} - 2z_-2\right) \\ \quad -(D_+^{-1} - D_-^{-1})^2\left(-\dfrac{z_+^2(z_+ + z_-)(z_+ - z_-)^2}{z_-} + z_+^2z_-^2\left(1 + \dfrac{z_+}{z_-}\right)^2 + \dfrac{z_+^4}{z_+ - z_-}\left(1 + \dfrac{z_+}{z_-}\right)^2\right) \end{array}\right) \\ \quad + \dfrac{\mathrm{i}\omega^3}{\kappa^6 D_+^3 D_-^3(z_+ - z_-)}\left[\begin{array}{l} \left(\left(\dfrac{2z_-}{(z_+ - z_-)}\right) + \dfrac{z_+}{z_-}\left(\begin{array}{l} \dfrac{z_-^2}{(z_+ - z_-)}\left(\dfrac{(D_- - D_+)z_+}{z_-}\right)\left(-2 + 2z_+ + \dfrac{(D_- - D_+)^2(z_- + z_+)^2}{(z_- - z_+)}\right) \\ \quad + \left(\dfrac{2z_+(D_- - D_+)(z_- + z_+)(z_-D_-^2 - z_+D_+^2)}{(z_- - z_+)}\right) \end{array}\right)\right) \\ +(D_- - D_+)(z_- + z_+)(z_-D_-^{-2} - z_+D_+^{-2})\left(\dfrac{2z_-}{(z_+ - z_-)} - \dfrac{z_+}{z_-}\right) \\ +2z_-(D_- + D_+)(z_-D_-^2 - z_+D_+^2) - \left(\dfrac{z_-^2(D_- - D_+)(z_- + z_+)}{(z_+ - z_-)}\right) \\ \times\left(-2 - \dfrac{2z_+}{z_-} - \dfrac{z_-}{z_+ - z_-}\left(\dfrac{(D_- - D_+)(z_- + z_+)}{z_-}\right)^2\right)\left(1 + \dfrac{1}{z_-^2}\right) \end{array}\right] \end{array}\right]. \tag{A40}$$

References

[1] Hussain S, Youngs I J and Ford I J 2004 *J. Phys. D: Appl. Phys.* **37** 318

[2] Lyklema J, Van Leeuwen H P and Minor M 1999 *Adv. Colloid Interface Sci.* **83** 33

[3] O'Brien R W 1986 *J. Colloid Interface Sci.* **113** 81

[4] Craig D Q M 1995 *Dielectric Analysis of Pharmaceutical Systems* (London: Taylor and Francis)

[5] Chassagne C, Bedeaux D and Koper G J M 2001 *J. Phys. Chem.* **105** 11743

[6] Grosse C, Tirado M, Pieper W and Pottel R 1998 *J. Colloid Interface Sci.* **205** 26

[7] Atkins P W 1999 *Physical Chemistry* (Oxford: Oxford University Press)

[8] Russell A S, Scales P J, Mangelsdorf C S and White L R 1995 *Languir* **11** 1553

[9] Hunter R J 1992 *Foundations of Colloid Science* (Oxford: Oxford University Press)

[10] Pitman K C, Lindley M W, Simkin D and Cooper J F 1991 *IEE Proc.* F **138** (3) 223